3

Coverage Self-optimization for Randomly Deployed Indoor Small Cell Networks

In terms of the coverage problem in small cell networks, a joint coverage self-optimization scheme has been proposed by using the artificial neural networks model to improve the coverage performance in this chapter. First, the problems and challenges for the randomly deployed small cell networks have been summarized in the indoor scenario. Then, the theoretical models are proposed for the optimal coverage radius modelling in three typical indoor locations, such as the center position, corner position, and the sidewall midpoint position. Moreover, the optimal power allocation schemes for the indoor small cell networks are proposed with theoretical results and analyses. At last, the artificial neural networks model based joint coverage self-optimization scheme has been proposed and the performances of proposed schemes are verified by numerous results in this chapter.

3.1 Introduction of Problems and Challenges

According to recent studies, about 50% of phone calls and 70% of data services will take place indoors in the coming years [1]. However, it has been noticed that more than 45% of households and 30% of businesses experience inadequate indoor coverage [2], which often results in the poor QoS. To meet these increasing service demands, new techniques to improve the indoor coverage are needed.

To solve the problem of poor indoor coverage, several techniques have been already developed in the literature [3]. For example, outdoor macro or micro base stations with increased transmit power have been deployed to enhance the indoor coverage. However, these solutions provide limited performance enhancements due to the increased inter-cell interference and the high penetration loss through walls. The effect of the location of antennas indoors should also be considered to improve the received signal power. A distributed antenna system (DAS) [4] with multiple antennas located on different floors and a radiating or leaky cable along

corridors are two candidate approaches for indoor coverage enhancements. Although these techniques can improve the indoor coverage, the precise network planning with appropriate optimization is required to limit or mitigate interferences. Moreover, in a home environment, these techniques may not be applicable or desirable due to privacy issues.

A better approach is to deploy small scale femtocell base stations (FBSs) or home node Bs (HNBs) that have been designed for indoor coverage [5]-[7]. A user deployed FBS is a short-range, low-cost, and low-power solution which can provide a guaranteed QoS for voice and high-speed data services in home, office or other indoor environments. And the FBS can easily be connected to a digital subscriber line (DSL) or cable modem. As wireless bandwidth resources are scarce [8], FBSs sharing the same spectrum with macrocell BSs is an acceptable and efficient way of improving the indoor coverage and the network capacity. However, considering that FBSs are typically deployed randomly indoors by users without any network planning or centralized optimization, it is essential to apply the self-organizing techniques [3] [9] [10], to ensure the effective FBS implementation in a Plug-and-Play (PnP) manner.

The potentially large number of randomly deployed FBSs makes indoor coverage self-optimization a big challenge. Thus, the main focus of this work is to answer the following questions. (1) Does the optimal coverage radius exist for indoor FBSs? (2) What parameters will have a significant effect on FBS indoor coverage optimization? (3) How can self-optimization be achieved intelligently and efficiently?

By solving these questions, the problem of indoor coverage self-optimization will be explored by a realistic randomly deployed FBS environment. In the literature, both indoor coverage optimization and interference mitigation for FBSs have been investigated, which include the distributed power control

mechanisms, switched multi-element antennas techniques, and auto-configuration schemes.

Considering the increased size and complexity of femtocell networks, the joint distributed coverage optimization scheme has been proposed in [11] in terms of pilot transmit (TX) power, user load, and coverage holes. But this scheme only considered about the rudimentary planned enterprise femtocell networks. Furthermore, an eICIC method based on a tighter coordination between macro and femto nodes is proposed by using an effective autonomous power control algorithm in [12]. A distributed and self-organizing femtocell management architecture called the Complementary TRi-control Loops (CTRL) is also proposed in terms of the maximum transmit power and SINR in [13]. However, these algorithms have not considered about the randomly deployed characteristics of FBSs in the indoor environment. A distributed utility-based SINR adaptation technique for femtocells is proposed in [14] by reducing the Tx power of the strongest co-channel femtocell interferers to limit the interference to the macrocell. But it neglects the effects of FBS's indoor locations and its antenna patterns to the interference increase. Moreover, the interference management techniques for both downlink (DL) and uplink (UL) in femtocell networks are proposed in [15]. Using both fixed and adaptive thresholds based on the noise and interference at the macrocell base station (MBS), both open and closed loop control interference mitigation strategies are proposed in [16]. Two distributed power control mechanisms, namely geostatic and adaptive power control, are proposed in [17] to provide a balance between the throughput of femtocell users and the macrocell performance degradation. However, these techniques assume that FBSs are placed in the specific pre-defined indoor locations, which neglects the coverage and interference issues caused by randomly deployed FBSs in homes and offices.

Auto-configuration of both the pilot and Tx power for each femtocell in the co-channel environment is proposed in [18] to achieve a constant femtocell range in the DL and a low macrocell interference level in the UL. However, it only takes into account the signal received from the closest macrocell, but neglects the interference from neighbour femtocells. Auto-configuration and power control adaptation techniques for femtocells in a co-channel environment are investigated in [19] by evaluating the handover and dropped call probabilities of macrocell users. Furthermore, the 3rd Generation Partnership Project (3GPP) and 3GPP2 have also examined femtocells issues in [20]-[21], including system architecture, interfaces and protocols, self-configuration and self-optimization.

As a coverage optimization scheme, switched multi-element antennas has been proved to be effective to improve the indoor coverage [22]. Multiple antenna techniques have also been developed to enhance the robustness against the near-far problem and maximize the number of femtocell users for the simultaneous transmission under outage probability constraints in [23]. However, the joint power allocation and antenna pattern design, particularly for randomly deployed indoor FBSs, has not been studied yet.

Although the coverage optimization and interference mitigation schemes have been proposed in the literature, the randomly deployed FBSs indoors create new challenges for the coverage optimization and interference mitigation which have never been discussed before. Thus, an artificial neural network (ANN) model for joint coverage self-optimization has been proposed in this chapter to solve these challenges by using the intelligent parameter optimization and tuning technologies [33]. Results prove that the optimal coverage radius exists for the indoor FBS in typical positions, such as the center, corner, and midpoint of a sidewall. Moreover, a dynamic power allocation scheme is applied to minimize the interference caused by the FBS to the MBS and neighbour macrocell users. Based on the proposed dynamic power allocation technique, a joint dynamic

power allocation and antenna pattern selection scheme is further designed which utilizes the FBS position information. Moreover, ANN model is used for the intelligent coverage self-optimization, which provides a practical and efficient solution for the PnP of FBS regardless of its position.

3.2 Theoretical Model and Analysis on Optimal Coverage Radius

Considering the scenario of user-deployed FBS without careful network planning, it will cause indoor coverage holes and outdoor interferences, which is a big challenge unsolved so far. Therefore, the existence of optimal coverage radius is proved for indoor FBSs in typical positions. A coverage hole is defined as an area in which the received signal strength is below the threshold required for a given service. To simplify the analysis, it is assumed that the room is square with the wall lengths D_s m and the FBS location resolution is 1 m^2, so there are D_s^2 possible FBS locations. The area of the indoor coverage holes and the outdoor interference range are defined as δ_{ICH} and δ_{OI}, respectively. Therefore, a typical scenario with one FBS randomly deployed indoors is shown in Figure 3.1. And the optimal FBS coverage radii exist and are proved below including the center, corner, and midpoint positions.
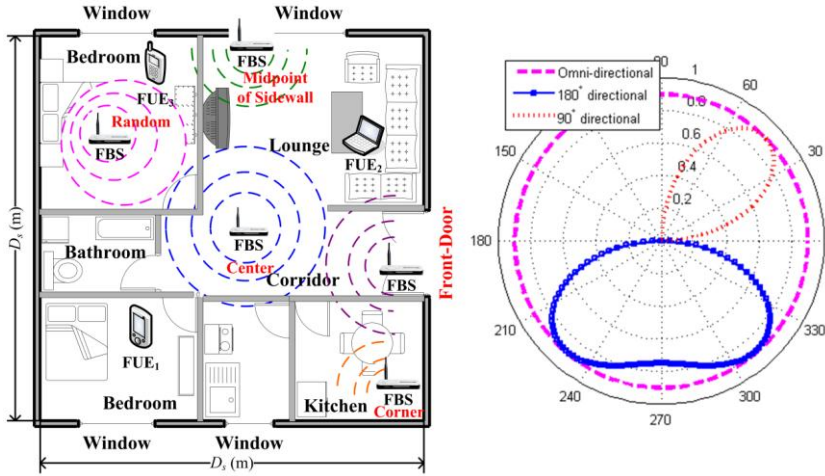
Figure 3.1 *Randomly deployed FBS in a room for three typical antenna patterns (omni, 180◦ and 90◦). SOURCE: Reproduced with permission from [33]. Copyright 2015 Springer US.*

3.2.1 Optimal Coverage Radius for Center Position

The indoor coverage holes and outdoor interference range are shown in Figure 3.1 for different values of R_f and D_s when the FBS is located in the center position.

The values of δ_{ICH} and δ_{OI} are calculated below under different conditions in Figure 3.2.

1) When $0 < R_f \leq D_s / 2$, δ_{ICH} is given by (1) and $\delta_{OI} = 0$.

$$\delta_{ICH} = (D_s^2 - \pi R_f^2) / D_s^2 \tag{1}$$

2) When $D_s / 2 < R_f < \sqrt{2} D_s / 2$, δ_{ICH} and δ_{OI} are given by (2) and (3).

$$\delta_{ICH} = \frac{8}{D_s^2}(S_{OCB} - S_{OFB})$$

$$= \frac{1}{D_s^2}\left[D_s^2 - D_s\sqrt{4R_f^2 - D_s^2} - \pi R_f^2 + 4R_f^2 \arccos\left(\frac{D_s}{2R_f}\right) \right] \tag{2}$$

$$\delta_{OI} = \frac{8}{D_s^2}\left(S_{OBD} - S_{OBA}\right)$$

$$= \frac{1}{D_s^2}\left[4R_f^2 \arccos\left(\frac{D_s}{2R_f}\right) - D_s\sqrt{4R_f^2 - D_s^2} \right] \tag{3}$$

Where $\angle AOB = \alpha = \arccos(D_s / 2R_f)$, $\angle BOC = \beta = \pi / 4 - \alpha$, $0 < \alpha, \beta < \pi / 4$.

3) When $R_f \geq \sqrt{2}D_s / 2$, $\delta_{ICH} = 0$ and δ_{OI} is given by (4).

$$\delta_{OI} = (\pi R_f^2 - D_s^2) / D_s^2 \tag{4}$$

Thus, δ_{ICH} and δ_{OI} are given by (5) and (6) briefly.

$$\delta_{ICH} = \begin{cases} D_s^2 - \pi R_f^2 / D_s^2 & 0 < R_f \leq D_s / 2 \\ \frac{1}{D_s^2}\left[D_s^2 - D_s\sqrt{4R_f^2 - D_s^2} - \pi R_f^2 + 4R_f^2 \arccos\left(\frac{D_s}{2R_f}\right) \right] & D_s / 2 < R_f < \sqrt{2}D_s / 2 \\ 0 & R_f \geq \sqrt{2}D_s / 2 \end{cases} \tag{5}$$

$$\delta_{OI} = \begin{cases} 0 & 0 < R_f \leq D_s / 2 \\ \frac{1}{D_s^2}\left[4R_f^2 \arccos\left(\frac{D_s}{2R_f}\right) - D_s\sqrt{4R_f^2 - D_s^2} \right] & D_s / 2 < R_f < \sqrt{2}D_s / 2 \\ (\pi R_f^2 - D_s^2) / D_s^2 & R_f \geq \sqrt{2}D_s / 2 \end{cases} \tag{6}$$

Based on (5) and (6), the optimal coverage radius problem transforms to determine the optimal FBS coverage radius R_f^{Opt} in (7) with conditions in (8).

$$R_f^{Opt} = \arg \min \delta \qquad (7)$$

$$\delta = \begin{cases} D_s^2 - \pi R_f^2 / D_s^2 & 0 < R_f \leq D_s/2 \\ \dfrac{1}{D_s^2} \left[D_s^2 - 2D_s\sqrt{4R_f^2 - D_s^2} - \pi R_f^2 + 8R_f^2 \arccos\left(\dfrac{D_s}{2R_f}\right) \right] & D_s/2 < R_f < \sqrt{2}D_s/2 \\ (\pi R_f^2 - D_s^2)/D_s^2 & R_f \geq \sqrt{2}D_s/2, \end{cases} \qquad (8)$$

Where $\delta = (\delta_{ICH} + \delta_{OI})$ is the sum of the coverage holes and the interference range.

Therefore, the minimum value of δ is $\delta^{\min} = \min(\delta_1^{\min}, \delta_2^{\min}, \delta_3^{\min}) = \delta_2^{\min} = 0.17$ with an optimal FBS coverage radius of $R_f^{Opt} = \arg \min \delta = 0.54 D_s$, as shown in Figure 3.2.
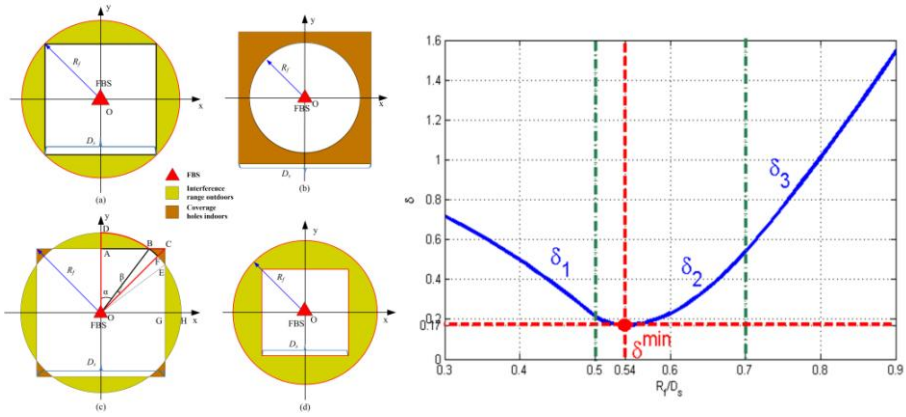
Figure 3.2 *Optimal R_f for FBS in the center position. SOURCE: Reproduced with permission from [33]. Copyright 2015 Springer US.*

3.2.2 Optimal Coverage Radius for Corner Position

The indoor coverage holes and outdoor interference range for FBS located in the corner position are shown in Figure 3.3 for different values of R_f and D_s.

Similar to the analysis of center position scenario, the optimal coverage radius is calculated for both δ_{ICH} and δ_{OI} below.

1) When $0 < R_f \le D_s$, δ_{ICH} is given by (9) and $\delta_{OI} = 0$.

$$\delta_{ICH} = (D_s^2 - \pi R_f^2 / 4) / D_s^2 \tag{9}$$

2) When $D_s < R_f < \sqrt{2}D_s$, δ_{ICH} and δ_{OI} are given by (10) and (11).

$$
\begin{aligned}
\delta_{ICH} &= \frac{2}{D_s^2}\left(S_{OCB} - S_{OFB}\right) \\
&= \frac{1}{D_s^2}\left[D_s^2 - D_s\sqrt{R_f^2 - D_s^2} - \frac{\pi}{4}R_f^2 + R_f^2 \arccos\left(\frac{D_s}{R_f}\right)\right]
\end{aligned}
\tag{10}
$$

$$
\begin{aligned}
\delta_{OI} &= \frac{2}{D_s^2}\left(S_{OBD} - S_{OBA}\right) \\
&= \frac{1}{D_s^2}\left[R_f^2 \arccos\left(\frac{D_s}{R_f}\right) - D_s\sqrt{R_f^2 - D_s^2}\right]
\end{aligned}
\tag{11}
$$

Where $\angle AOB = \alpha = \arccos(D_s / R_f)$, $\angle BOC = \beta = \pi / 4 - \alpha$, $0 < \alpha, \beta < \pi / 4$.

3) When $R_f \ge \sqrt{2}D_s$, $\delta_{ICH} = 0$ and δ_{OI} is given by (12).

$$\delta_{OI} = (\pi R_f^2 / 4 - D_s^2) / D_s^2 \tag{12}$$

Thus, δ_{ICH} and δ_{OI} are given by (13) and (14) briefly.

$$\delta_{ICH} = \begin{cases} (D_s^2 - \pi R_f^2/4)/D_s^2 & 0 < R_f \le D_s \\ \dfrac{1}{D_s^2}\left[D_s^2 - D_s\sqrt{R_f^2 - D_s^2} - \dfrac{\pi}{4}R_f^2 + R_f^2 \arccos\left(\dfrac{D_s}{R_f}\right) \right] & D_s < R_f < \sqrt{2}D_s \\ 0 & R_f \ge \sqrt{2}D_s \end{cases} \qquad (13)$$

$$\delta_{OI} = \begin{cases} 0 & 0 < R_f \le D_s \\ \dfrac{1}{D_s^2}\left[R_f^2 \arccos\left(\dfrac{D_s}{R_f}\right) - D_s\sqrt{R_f^2 - D_s^2} \right] & D_s < R_f < \sqrt{2}D_s \\ (\pi R_f^2/4 - D_s^2)/D_s^2 & R_f \ge \sqrt{2}D_s \end{cases} \qquad (14)$$

Based on (13) and (14), the optimal coverage radius problem transforms to determine the optimal FBS coverage radius R_f^{Opt} in (7) with conditions in (15), where $\delta = (\delta_{ICH} + \delta_{OI})$.

$$\delta = \begin{cases} (D_s^2 - \pi R_f^2/4)/D_s^2 & 0 < R_f \le D_s \\ \dfrac{1}{D_s^2}\left[D_s^2 - 2D_s\sqrt{R_f^2 - D_s^2} - \dfrac{\pi}{4}R_f^2 + 2R_f^2 \arccos\left(\dfrac{D_s}{R_f}\right) \right] & D_s < R_f < \sqrt{2}D_s \\ (\pi R_f^2/4 - D_s^2)/D_s^2 & R_f \ge \sqrt{2}D_s, \end{cases} \qquad (15)$$

Therefore, the minimum δ is $\delta^{\min} = \min(\delta_1^{\min}, \delta_2^{\min}, \delta_3^{\min}) = \delta_2^{\min} = 0.17$ with an optimal FBS coverage radius of $R_f^{Opt} = \arg\min \delta = 1.08 D_s$, as shown in Figure 3.3.
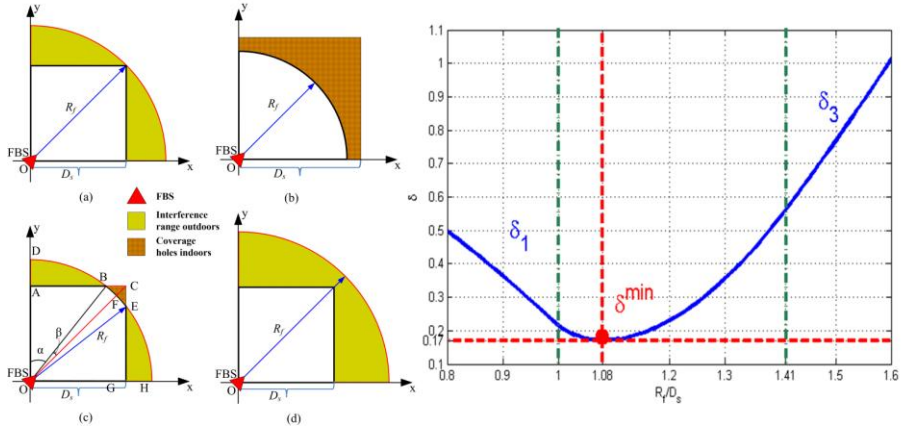
Figure 3.3 *Optimal R_f for FBS in the corner position. SOURCE: Reproduced with permission from [33]. Copyright 2015 Springer US.*

3.2.3 Optimal Coverage Radius for Sidewall Midpoint Position

The indoor coverage holes and outdoor interference range for FBS located at the midpoint of the sidewall are shown in Figure 3.4 for different values of R_f and D_s. Similar to the above analysis, the optimal coverage radius is calculated for both δ_{ICH} and δ_{OI} below.

1) When $0 < R_f \leq D_s / 2$, $\delta_{OI} = 0$ and δ_{ICH} is given by (16).

$$\delta_{ICH} = (D_s^2 - \pi R_f^2 / 2) / D_s^2 \tag{16}$$

2) When $D_s / 2 < R_f < D_s$, δ_{ICH} and δ_{OI} are given by (17) and (18).

$$\begin{aligned}
\delta_{ICH} &= \frac{2}{D_s^2} \left(S_{OGBD} - S_{OGE} - S_{OEA} \right) \\
&= \frac{1}{D_s^2} \left[D_s^2 - \frac{D_s}{4} \sqrt{4R_f^2 - D_s^2} - \frac{\pi}{2} R_f^2 + R_f^2 \arccos\left(\frac{D_s}{2R_f} \right) \right]
\end{aligned} \tag{17}$$

$$\begin{aligned}
\delta_{OI} &= \frac{2}{D_s^2}\left(S_{OHE} - S_{OGE}\right) \\
&= \frac{1}{D_s^2}\left(R_f^2 \arccos\left(\frac{D_s}{2R_f}\right) - \frac{D_s}{4}\sqrt{4R_f^2 - D_s^2}\right)
\end{aligned} \tag{18}$$

Where $\angle GOE = \alpha = \arccos[D_s/(2R_f)]$, $\angle AOE = \beta = \pi/2 - \alpha$, $0 < \alpha < \pi/3$.

3) When $D_s \leq R_f < \sqrt{5}D_s/2$, δ_{ICH} and δ_{OI} are given by (19) and (20).

$$\begin{aligned}
\delta_{ICH} &= \frac{2}{D_s^2}\left(S_{OGCA} - S_{OGE} - S_{OBA} - S_{OFB} - S_{OEF}\right) \\
&= \frac{1}{D_s^2}\left[D_s^2 - \frac{D_s}{4}\sqrt{4R_f^2 - D_s^2} - D_s\sqrt{R_f^2 - D_s^2} - \frac{\pi}{2}R_f^2 + R_f^2\arccos\left(\frac{D_s}{R_f}\right) + R_f^2\arccos\left(\frac{D_s}{2R_f}\right)\right]
\end{aligned} \tag{19}$$

$$\begin{aligned}
\delta_{OI} &= \frac{2}{D_s^2}\left(S_{OHE} + S_{OBD} - S_{OGE} - S_{OBA}\right) \\
&= \frac{1}{D_s^2}\left[R_f^2\arccos\left(\frac{D_s}{2R_f}\right) + R_f^2\arccos\left(\frac{D_s}{R_f}\right) - \frac{D_s}{4}\sqrt{4R_f^2 - D_s^2} - D_s\sqrt{R_f^2 - D_s^2}\right]
\end{aligned} \tag{20}$$

Where $\angle BOA = \alpha = \arccos(D_s/R_f)$, $\angle BOC = \beta = \arctan(1/2) - \alpha$, $\angle GOE = \mu = \arccos[D_s/(2R_f)]$, $\angle EOC = \gamma = \arctan(2) - \mu$, $0 \leq \alpha < \arctan(1/2)$, $\pi/3 \leq \mu < \arctan(2)$.

4) When $R_f \geq \sqrt{5}D_s/2$, $\delta_{ICH} = 0$ and δ_{OI} is given by (21).

$$\delta_{OI} = (\pi R_f^2/2 - D_s^2)/D_s^2 \tag{21}$$

Thus, δ_{ICH} and δ_{OI} are given by (22) and (23) briefly.

$$\delta_{ICH} = \begin{cases} (D_s^2 - \pi R_f^2 / 2) / D_s^2 & 0 < R_f \le D_s / 2 \\[2mm] \dfrac{1}{D_s^2} \left[D_s^2 - \dfrac{D_s}{4}\sqrt{4R_f^2 - D_s^2} - \dfrac{\pi}{2}R_f^2 + R_f^2 \arccos\left(\dfrac{D_s}{2R_f}\right) \right] & D_s / 2 < R_f < D_s \\[4mm] \dfrac{1}{D_s^2} \left[\begin{array}{l} D_s^2 - \dfrac{D_s}{4}\sqrt{4R_f^2 - D_s^2} - D_s\sqrt{R_f^2 - D_s^2} - \dfrac{\pi}{2}R_f^2 \\[2mm] + R_f^2 \arccos\left(\dfrac{D_s}{R_f}\right) + R_f^2 \arccos\left(\dfrac{D_s}{2R_f}\right) \end{array} \right] & D_s \le R_f < \sqrt{5}D_s / 2 \\[4mm] 0 & R_f \ge \sqrt{5}D_s / 2 \end{cases} \tag{22}$$

$$\delta_{OI} = \begin{cases} 0 & 0 < R_f \le D_s / 2 \\[2mm] \dfrac{1}{D_s^2} \left(R_f^2 \arccos\left(\dfrac{D_s}{2R_f}\right) - \dfrac{D_s}{4}\sqrt{4R_f^2 - D_s^2} \right) & D_s / 2 < R_f < D_s \\[4mm] \dfrac{1}{D_s^2} \left[\begin{array}{l} R_f^2 \arccos\left(\dfrac{D_s}{2R_f}\right) + R_f^2 \arccos\left(\dfrac{D_s}{R_f}\right) \\[2mm] - \dfrac{D_s}{4}\sqrt{4R_f^2 - D_s^2} - D_s\sqrt{R_f^2 - D_s^2} \end{array} \right] & D_s \le R_f < \sqrt{5}D_s / 2 \\[4mm] (\pi R_f^2 / 2 - D_s^2) / D_s^2 & R_f \ge \sqrt{5}D_s / 2 \end{cases} \tag{23}$$

Based on (22) and (23), the optimal coverage radius problem transforms to determine the optimal FBS coverage radius R_f^{Opt} in (7) with the minimum sum δ in (24), where $\delta = (\delta_{ICH} + \delta_{OI})$.

$$\delta = \begin{cases} (D_s^2 - \pi R_f^2 / 2) / D_s^2 & 0 < R_f \le D_s / 2 \\ \dfrac{1}{D_s^2}\left[D_s^2 - \dfrac{D_s}{2}\sqrt{4R_f^2 - D_s^2} - \dfrac{\pi}{2}R_f^2 + 2R_f^2 \arccos\left(\dfrac{D_s}{2R_f}\right)\right] & D_s / 2 < R_f < D_s \\ \dfrac{1}{D_s^2}\left[\begin{array}{l} D_s^2 - \dfrac{D_s}{2}\sqrt{4R_f^2 - D_s^2} - 2D_s\sqrt{R_f^2 - D_s^2} - \dfrac{\pi}{2}R_f^2 \\ + 2R_f^2 \arccos\left(\dfrac{D_s}{R_f}\right) + 2R_f^2 \arccos\left(\dfrac{D_s}{2R_f}\right) \end{array}\right] & D_s \le R_f < \sqrt{5}D_s / 2 \\ (\pi R_f^2 / 2 - D_s^2) / D_s^2 & R_f \ge \sqrt{5}D_s / 2, \end{cases} \tag{24}$$

Therefore, the minimum value of δ is then $\delta^{\min} = \min(\delta_1^{\min}, \delta_2^{\min}, \delta_3^{\min}, \delta_4^{\min}) = \delta_2^{\min} = 0.5$ with an optimal FBS coverage radius of $R_f^{Opt} = \arg\min \delta = 0.71 D_s$, as shown in Figure 3.4.
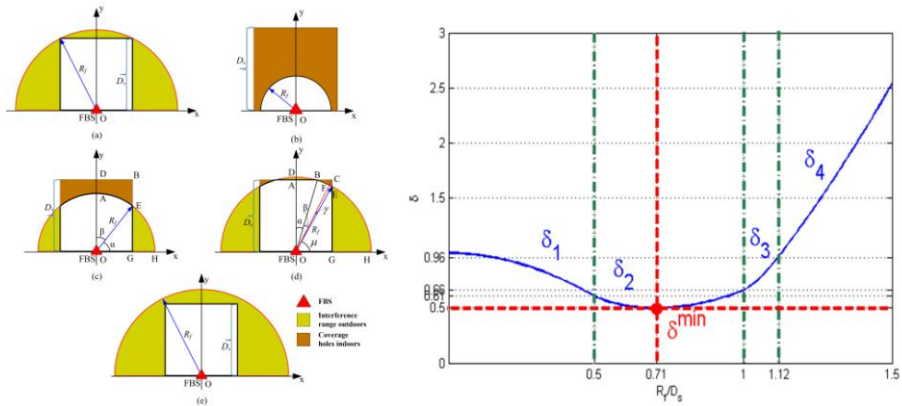
Figure 3.4 *Optimal* R_f *for FBS in the sidewall midpoint position. SOURCE: Reproduced with permission from [33]. Copyright 2015 Springer US.*

Furthermore, based on the analysis and results above, the optimal FBS coverage radii exist in three typical positions in Figure 3.1. In order to achieve the optimal radii to improve FBS's performance, the appropriate antenna pattern selection is also a key technology that should be applied in different positions. An omni-directional antenna pattern is preferred for FBS in the center position, a

$90°$ directional antenna for the corner position, and a $180°$ directional antenna for the sidewall midpoint position. For other FBS positions, a switched multi-element antenna [22] can be employed to obtain an appropriate antenna pattern to optimize FBS's coverage and its performance.

3.3 Optimal Power Allocation Scheme for Indoor Small Cell Networks

Moreover, in order to minimize the interference caused by indoor FBS due to the inappropriate power allocation scheme, different power allocation schemes are compared and analyzed in this section. In face of the randomly-deployed manner of FBS in homes and offices, the coverage self-optimization ability is indispensable for the optimal FBS deployment. Therefore, the coverage self-optimization scheme model is proposed and described first in this section. Then, both the static and dynamic power allocation schemes are proposed and compared thoroughly.

3.3.1 Coverage Self-optimization Scheme

The system model for FBS coverage self-optimization is shown in Figure 3.5. The effective coverage radii for FBS and MBS are r_A and d_C, respectively, centered at points A and C. The FBS interference radius is defined as r_C. Without an appropriate power allocation scheme, the indoor FBS signal may interfere to nearby outdoor MUE. Similarly, the outdoor MBS signal may interfere to indoor FUE. It is also assumed that the penetration loss for an interfering signal only depends on the obstacle material, i.e., glass, concrete, etc. The receiver noise is omitted for simplicity as the system is interference limited. Therefore, the FUE Signal-to-Interference-Ratio (SIR) at location A is given by (25) in [25].

$$SIR_{FUE}(r_A) = \frac{P_f / PL_f(r_A)}{G(\theta)P_m / PL_m(d_A) / L_w} \geq \Gamma_{target} \tag{25}$$

Where P_f is FBS's Tx power, $PL_f(r_A)$ is the path loss of FBS's signal at A, $G(\theta)$ is MBS's antenna gain [18] [22], P_m is MBS's Tx power, $PL_m(d_A)$ is the path loss of MBS's signal at A, L_w is the penetration loss through obstacles, and Γ_{target} is the minimum SIR value. The SIR of FUE in (25) can be expressed in decibels (dB) as (26).

$$SIR_{FUE}(r_A) = P_f - PL_f(r_A) - \left[P_m + G(\theta) - PL_m(d_A) - L_w \right] \geq \Gamma_{target} \tag{26}$$

Similarly, the SIR of MUE at the effective coverage range edge (point C in Figure 3.5) is depicted in (27).

$$SIR_{MUE}(d_C) = \frac{G(\theta)P_m / PL_m(d_C)}{P_f / PL_f(r_C) / L_w} \geq \Gamma_{target} \tag{27}$$

And the SIR of MUE can be expressed in dB as (28).

$$SIR_{MUE}(d_C) = P_m + G(\theta) - PL_m(d_C) - \left[P_f - PL_f(r_C) - L_w \right] \geq \Gamma_{target} \tag{28}$$

Manipulation of (26) and (28) gives the results in (29).

$$\begin{array}{rcl} -PL_f(r_A) + PL_m(d_A) & = & m - n \\ PL_f(r_C) - PL_m(d_C) & = & m + n \\ r_A + d_A = r_C + d_C & = & D_{MF} \end{array} \tag{29}$$

Where the path loss models of FBS and MBS are $PL_f(r) = 38.5 + 20\log_{10} r$ and $PL_m(d) = 28 + 35\log_{10} d$, respectively [18]-[22], D_{MF} is the distance between MBS and FBS, $m = \Gamma_{target} - L_w$ and $n = P_f - P_m - G(\theta)$.
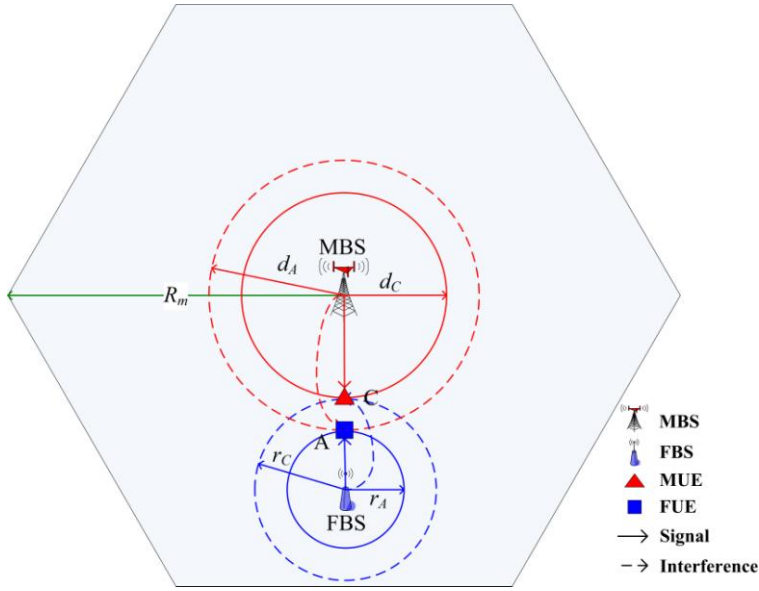
Figure 3.5 *The coverage self-optimization environment. SOURCE: Reproduced with permission from [33]. Copyright 2015 Springer US.*

3.3.2   Static Power Allocation Scheme

With the static power allocation (StPA), the FBS employs the maximum Tx power P_f for the signal transmission in order to meet the indoor coverage requirements. As a consequence, the DL signal from MBS will have a greater path loss due to its larger distance D_{MF}. Conversely, the path loss for the DL signal from the FBS is negligible indoors considering the small coverage area and short transmission distance. Let $P_f = 0.1\,\mathrm{W}$ (20 dBm), $P_m = 20\,\mathrm{W}$ (43 dBm) [24], $G(\theta) = 15dB$, $\Gamma_{target} = 5$ dB, $L_w = 1$ dB for glass, $m = 4$ dB, and

$n = 38\,\text{dB}$ from (29). The effective coverage radius of FBS is assumed to be $r_A = R_f = 10\,\text{m}$, so the MBS interference range radius is given by (30).

$$d_A = 10^{\frac{m-n+38.5-28+20\log_{10} r_A}{35}} \tag{30}$$

Thus, $d_A = 117\,\text{m}$ and $D_{MF} = r_A + d_A = 127\,\text{m}$. Therefore, $PL_f(r_C) - PL_m(d_C) = \Gamma_{target} - L_w + P_f - P_m - G(\theta)$. Based on (29), the results are shown in (31), where $r_c = 22\,\text{m}$ and $d_c = 105\,\text{m}$.

$$\begin{aligned}
&20\log_{10}(r_C) - 35\log_{10}(D_{MF} - r_C)\\
&= \Gamma_{target} - L_w + P_f - P_m - G(\theta) - (38.5 - 28)
\end{aligned} \tag{31}$$

To meet the minimum SIR requirements of FUE at the FBS coverage edge, at least $D_{MF} = 127\,\text{m}$ is needed. Furthermore, to guarantee the FBS effective coverage radius of $R_f = 10\,\text{m}$, it requires that $P_f = 20\,\text{dBm}$. The MUE will suffer from the interference due to FBS signal leakage through openings, such as windows, leading to an effective MBS coverage radius of $d_C = 105\,\text{m}$, and an FBS interference radius of $r_C = 22\,\text{m}$. An increase in D_{MF} will increase the FBS interference radius r_C, and increase the effective MBS coverage radius d_C. Based on (31), the interference radius of FBS r_C will increase as D_{MF} increases according to the StPA scheme, as shown in Figure 3.6.
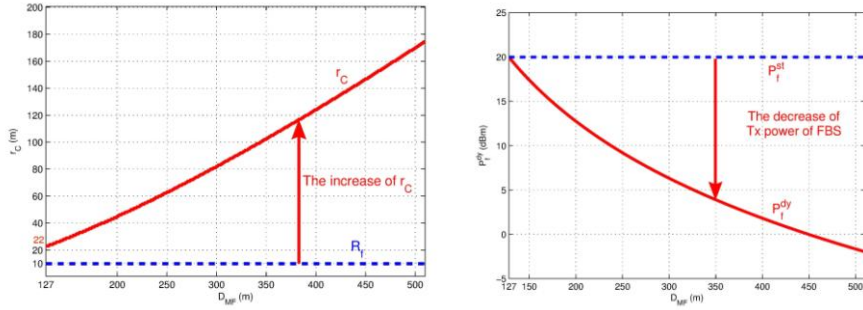
Figure 3.6 *FBS interference radius r_C and Tx power P_f^{dy} for the DyPA and StPA schemes. SOURCE: Reproduced with permission from [33]. Copyright 2015 Springer US.*

3.3.3   Dynamic Power Allocation Scheme

In order to decrease the interference caused by the StPA scheme in FBS, the dynamic power allocation (DyPA) is proposed to adaptively tune FBS's Tx power based on D_{MF}. The goal is to decrease the interference to nearby MUE while maintaining a good indoor coverage. To meet the minimum FUE SIR requirements at FBS's edge, the equation is depicted in (32)-(33).

$$-PL_f(r_A) + PL_m(d_A) = \Gamma_{target} - L_w - \left[P_f^{dy} - P_m - G(\theta) \right] \tag{32}$$

$$P_f^{dy} = \Gamma_{target} - L_w + PL_f(r_A) + P_m + G(\theta) - PL_m(d_A) \tag{33}$$

Because the interference from MBS to FUE decreases with the increase of D_{MF}, an FBS located far from the MBS can use a lower Tx power to provide the same coverage and guarantee the SIR for FUE indoors. Therefore, an FBS can employ the DyPA scheme to decrease the Tx power and reduce the interference to neighbour FUE. The Tx power P_f^{dy} of FBS employing DyPA is shown in Figure 3.6 versus D_{MF}. As D_{MF} increases, the FBS interference

radius r_C is controlled by using DyPA rather than StPA with $PL_f(r_C) - PL_m(d_C) = \Gamma_{target} - L_w + P_f^{dy} - P_m - G(\theta)$. Based on (29), the results are shown in (34).

$$20\log_{10}(r_C) - 35\log_{10}(D_{MF} - r_C)$$
$$= \Gamma_{target} - L_w + P_f^{dy} - P_m - G(\theta) - (38.5 - 28) \tag{34}$$

The interference radius r_C is controllable from 22 m to 26 m using the DyPA scheme, which is not sensitive to the increase of D_{MF}, as shown in Figure 3.7.

Considering the interference to MUE from FBS's signal, the effective MBS coverage radius d_C is given by $d_C = D_{MF} - r_C$. By employing the DyPA scheme at FBS, the interference can be decreased, which can greatly increases MBS's coverage radius d_C. Furthermore, considering the penetration loss through different obstacles, the MUE's interference from FBS differs, which will affect FBS's interference radius r_C and MBS's coverage radius d_C. Typical values of r_C and d_C are given in Table 3.1 for different penetration loss values L_w from 1 to 5 dB [3] when StPA is employed by FBS with $P_f = 20$ dBm. Since the FBS signal outdoors decreases as L_w increases, r_C will also decrease. Thus, MBS's coverage radius d_C also decreases as L_w increases. The FBS interference radius r_C and the MBS coverage radius d_C for different L_w are given in Figure 3.7 when StPA and DyPA are employed. This shows that as L_w increases, r_C and d_C decrease for the DyPA scheme in contrast to the StPA scheme. In addition, r_C stays constant with the increase of D_{MF} using the DyPA scheme. Note that d_C increases linearly with the

increase of D_{MF} using the DyPA scheme, so the effective coverage radius d_C is improved with the increase of L_w as the FBS interference is decreasing.
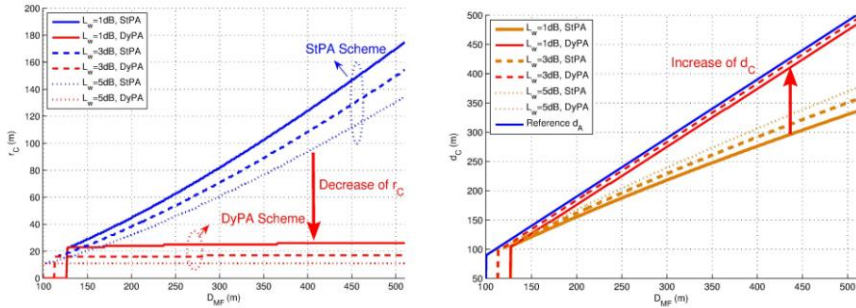
Figure 3.7 *MBS interference radius r_C and effective coverage radius d_C with different L_w for DyPA and StPA schemes. SOURCE: Reproduced with permission from [33]. Copyright 2015 Springer US.*

Table 3.1 *r_C and d_C for Different Penetration Loss Values L_w. SOURCE: Reproduced with permission from [33]. Copyright 2015 Springer US.*

L_w (dB)	1	2	3	4	5
$r_A = R_f$ (m)	10	10	10	10	10
d_A (m)	117	110	103	96	90
r_C (m)	22	19	15	13	10
d_C (m)	105	101	98	93	90
D_{MF} (m)	127	120	113	106	100

3.4 Artificial Neural Network Model Based Joint Coverage Self-optimization

In order to realize the coverage self-optimization in the randomly deployed FBS scenario, how to design an intelligent joint scheme by considering the coverage, power allocation, and antenna pattern effects is a big challenge.

Therefore, the artificial neural networks (ANNs) which have self-decision, intelligent learning, and self-adaptation characteristics, are appropriate for solving the joint power allocation and antenna pattern selection problem of randomly deployed FBS coverage self-optimization. The proposed ANN based approach employs training information from the optimal coverage radius results in typical FBS's positions, such as the center position, corner position, and the sidewall midpoint position.

3.4.1   Artificial Neural Network Model

Inspired by the structure of biological neural networks, ANNs are composed of many interconnected artificial neurons. They can be used to model complex relationships between inputs and outputs or to find patterns in a large data set by using the parallel data processing with a reasonable computational complexity. Therefore, ANNs are widely employed in pattern recognition, prediction, function approximation, classification, and adaptive control [26]-[27].

The artificial neuron model is shown in Figure 3.8(a), and consists of n input signals $x_1, x_2, \ldots, x_n$, n weights $w_{i1}, w_{i2}, \ldots, w_{in}$, a summation unit, a transfer function $f(x)$, and a threshold or bias θ_i. The output of this neuron is given by (35). And the possible transfer functions include the sign, linear and sigmoid (S-shaped) functions in [28].

$$y_i = f\left(\sum_{j=1}^{n} w_{ij} x_j - \theta_i\right) \tag{35}$$

Multiple neurons with the same input signal for parallel computing are called layers. The neurons with input and output connections form the multi-layer ANN, which consist of feedforward ANN and feedback ANN. Based on the back propagation (BP) learning algorithm [29]-[30], the coverage

self-optimization problem for random-deployed FBS can be modeled as a multi-layer feedforward neural network (MFNN) [31]-[32], which consists of three layers such as input layer, hidden layer, and output layer in Figure 3.8(b). Furthermore, based on the sequence training process, the MFNN based model for coverage self-optimization can be adaptive to the random locations of FBS indoors using the BP learning algorithm to update weights in different layers. Three key steps of the least mean square (LMS) algorithm used in the BP based MFNN model is described below.

1) Initialization: Choose the proper structure of ANN. And the number of neurons in the input, hidden, and output layers are depicted by p, l, q, respectively.

2) For the nth loop of the training process: Calculate the parameters based on the training sequence $x_1(n), x_2(n), \ldots, x_p(n)$ and the target output sequence $d_1(n), d_2(n), \ldots, d_q(n)$, as shown below.

i) Feedforward calculation process: The neuron j in the hidden layer satisfies the formulas in (36)-(37) and the neuron t in the output layer satisfies the formulas in (38)-(40), where $Net_j^{(1)}(n)$ and $Net_j^{(2)}(n)$ are the weighted sum of input signals in the hidden layer and the output layer, $x_i(n)$ is the input signal of neuron i in the input layer, $o_j(n)$ is the input signal of neuron j in the hidden layer, $y_t(n)$ is the output signal of neuron t in the output layer, $e_t(n)$ is the mean squared error (MSE) signal of neuron t in the output layer and the transfer function with S-shaped as $f_1(x) = f_2(x) = \left(1 + e^{-x}\right)^{-1}$.

$$Net_j^{(1)}(n) = \sum_{i=1}^{p} w_{ji}^{(1)} x_i(n) - \theta_j \tag{36}$$

$$o_j(n) = f_1(Net_j^{(1)}(n)) \tag{37}$$

$$Net_t^{(2)}(n) = \sum_{j=1}^{l} w_{tj}^{(2)} o_j(n) - \theta \tag{38}$$

$$y_t(n) = f_2(Net_t^{(2)}(n))_t \tag{39}$$

$$e_t(n) = d_t(n) - y_t(n) \tag{40}$$

ii) Calculate the MSE of the output layer in the nth loop in (41)-(42), where N is the sample period or the iteration of the training sequence. The learning process stops until the MSE value E of the output layer achieves the expected value, otherwise continues to step iii).

$$e(n) = \frac{1}{2} \sum_{t=1}^{q} e_t^2(n) \tag{41}$$

$$E = \sum_{n=1}^{N} e(n) \tag{42}$$

iii) Feedback calculation process of the local gradient δ: The gradient $\delta_t^{(2)}(n)$ of neuron t in the output layer satisfies the formulas in (43) and the gradient $\delta_t^{(1)}(n)$ of neuron j in the hidden layer satisfies the formulas in (44).

$$\begin{aligned}
\delta_t^{(2)}(n) &= -\frac{\partial e(n)}{\partial Net_t^{(2)}(n)} = -\frac{\partial e(n)}{\partial y_t(n)} \frac{\partial y_t(n)}{\partial Net_t^{(2)}(n)} \\
&= e_t(n) \frac{\partial y_t(n)}{\partial Net_t^{(2)}(n)} = [d_t(n) - y_t(n)] y_t(n)[1 - y_t(n)]
\end{aligned} \tag{43}$$

$$\delta_j^{(1)}(n) = -\frac{\partial e(n)}{\partial Net_j^{(1)}(n)} = -\frac{\partial e(n)}{\partial o_j(n)} \frac{\partial o_j(n)}{\partial Net_j^{(1)}(n)}$$

$$= -o_j(n)[1 - o_j(n)] \sum_{j=1}^{q} \frac{\partial e(n)}{\partial y_j(n)} \frac{\partial y_j(n)}{\partial Net_j^{(2)}(n)} \frac{\partial Net_j^{(2)}(n)}{\partial o_j(n)}$$

$$= o_j(n)[1 - o_j(n)] \sum_{j=1}^{q} [\delta_j^{(2)}(n) w_{tj}]$$

$$= o_j(n)[1 - o_j(n)] \sum_{j=1}^{q} \left\{ [d_j(n) - y_j(n)] y_j(n)[1 - y_j(n)] w_{tj} \right\} \tag{44}$$

iv) Revise the weights in three layers. The weights from neuron j in the hidden layer to neuron t in the output layer satisfies (45)-(46). And the weights from neuron i in the input layer to neuron j in the hidden layer satisfy the formulas in (47)-(48), where $\eta \in (0,1)$ is the learning step.

$$w_{tj}^{(2)}(n+1) = w_{tj}^{(2)}(n) + \Delta w_{tj}^{(2)}(n) \tag{45}$$

$$\Delta w_{tj}^{(2)}(n) = -\eta \frac{\partial e(n)}{\partial w_{tj}^{(2)}(n)}$$

$$= -\eta \frac{\partial e(n)}{\partial Net_t^{(2)}(n)} \frac{\partial Net_t^{(2)}(n)}{\partial w_{tj}^{(2)}(n)} = \eta \delta_t^{(2)}(n) o_j(n) \tag{46}$$

$$w_{ji}^{(1)}(n+1) = w_{ji}^{(1)}(n) + \Delta w_{ji}^{(1)}(n) \tag{47}$$

$$\Delta w_{ji}^{(1)}(n) = -\eta \frac{\partial e(n)}{\partial w_{ji}^{(1)}(n)}$$

$$= -\eta \frac{\partial e(n)}{\partial Net_j^{(1)}(n)} \frac{\partial Net_j^{(1)}(n)}{\partial w_{ji}^{(1)}(n)} = \eta \delta_j^{(1)}(n) x_i(n) \tag{48}$$

3) Set $n = n + 1$, and input another new sample sequence.

3.4.2   ANN Based Joint Coverage Self-optimization Scheme Design

For the ANN based joint coverage self-optimization, typical FBS locations and MBS to FBS distances are the input variables. The antenna patterns and Tx power allocations are the output variables. Both input and output variables are used in the training process to obtain the appropriate weights in three layers. The ANN with optimized weights as shown in Figure 3.8(c) is applied to solve the coverage self-optimization problem.

The indoor FBS's positions can be center, corner, sidewall midpoint, or random position, so two input parameters $\{x_1, x_2\}$ are used to identify different FBS's positions F_{pst}. Similarly, the distance between MBS and FBS is $D_{MF} < R_m = 500$ m, so nine input parameters are used to depict D_{MF}, namely $\{x_3, x_4, \ldots, x_{11}\}$, where the minimum distance resolution is 1 m. Two output parameters $\{y_1, y_2\}$ are used for the antenna patterns (e.g. omni-directional, 180° directional, and 90° directional). The maximum and minimum FBS's Tx power are assumed to be 20 dBm and -10 dBm, respectively, and five output parameters are used for different power levels $\{y_3, y_4, \ldots, y_7\}$. This allows for 31 power levels with a tunable step interval of 1 dBm. The number of neurons in the input and output layers is $p = 11$ and $q = 7$, respectively.
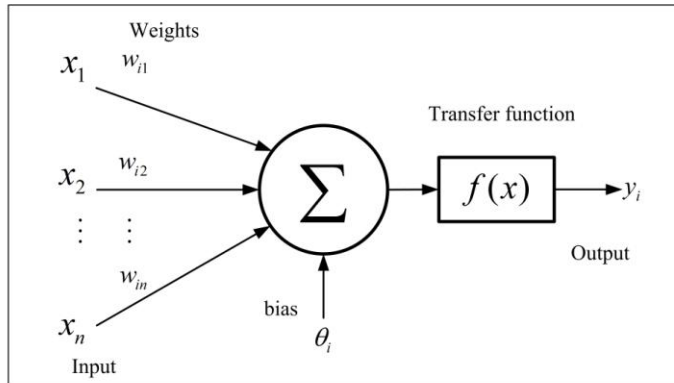
(a)
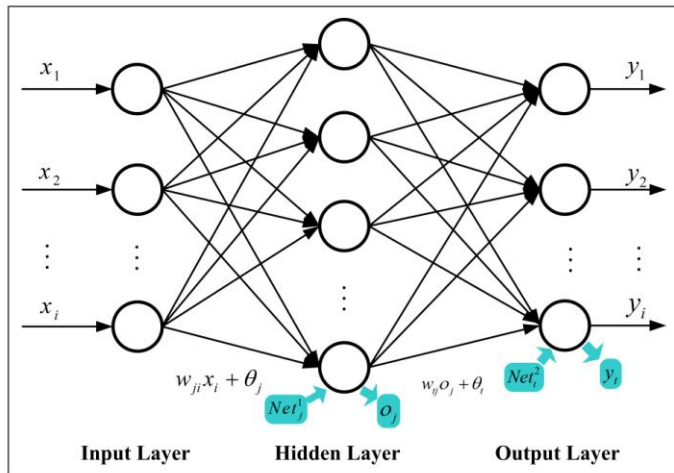
(b)
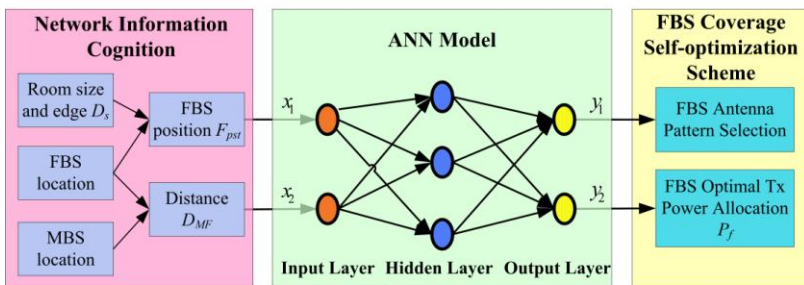
(c)

Figure 3. 8 *(a) Artificial neuron model, (b) three layer ANN model, and (c) ANN based FBS coverage self-optimization system. SOURCE: Reproduced with permission from [33]. Copyright 2015 Springer US.*

3.5 Results and Performance Analyses

The simulation environment is shown in Figure 3.9. The MBS is located at the origin $O(0,0)$ in Cartesian coordinates, and the FBS is at $F(x_f, y_f)$ of the center of a square house $H(x_h, y_h)$. The house sidewall lengths are $D_s = 10\,\text{m}$. The FBS position is shown in (49).

$$F_{pst}(x_1, x_2) = \begin{cases} 01 & (x_f, y_f) = (x_h, y_h) \\ 10 & (x_f, y_f) = (x_h \pm D_s / 2, y_h \pm D_s / 2) \\ 11 & (x_f, y_f) = (x_h, 0) \text{ or } (x_f, y_f) = (0, y_h) \\ 00 & \text{otherwise} \end{cases} \tag{49}$$

$F_{pst} = \{01, 10, 11, 00\}$ denotes the center, corner, sidewall midpoint, and random positions, respectively. $A_t^p = \{01, 10, 11\}$ denotes the omni-directional, 180◦ directional, and $90°$ directional FBS antenna patterns, respectively. For $F_{pst} = \{01, 10, 11, 00\}$, the optimal FBS coverage radius is given by $R_f / D_s = \{0.54, 1.08, 0.71, 1.41\}$ based on the analysis in Section 3.2. It is assumed that the coverage radius for a randomly deployed FBS satisfies $R_f = 1.41 D_s$. The key parameters for FBS coverage optimization are shown in Table 3.2.

The MBS interference range is calculated by using (30) where $r_A = R_f$. The minimum distance between MBS and FBS is $D_{MF}^{min} = d_A + R_f$. When $D_{MF} = \sqrt{x_f^2 + y_f^2} \geq D_{MF}^{min}$, the dynamic FBS power allocation P_f^{dy} is calculated using (33), where $-10\,\text{dBm} \leq P_f^{dy} \leq 20\,\text{dBm}$. Figure 3.10 shows how P_f^{dy} decreases as D_{MF} increases for different FBS positions. For the same value of

D_{MF}, different power allocation schemes are required to achieve the optimal FBS coverage with minimum interference to both MBS and MUE.

The ANN model has 11 neurons in the input layer, where FBS's position F_{pst} has 2 bits and the distance between MBS and FBS D_{MF} has 9 bits. There are 15 neurons in the hidden layer considering the complexity and accuracy of sequence training. And 7 neurons are designed in the output layer, where the antenna pattern A_t^p has 2 bits and FBS Tx power P_f^{dy} has 5 bits. For example, the input training sequence $X_1 = (01010010110)^T$ denotes that the FBS is located at the center position with a distance of 150 m to the MBS. An output $D_1 = (0110101)^T$ denotes that the FBS uses an omni-directional antenna pattern with the Tx power 11 dBm. Typical FBS positions and D_{MF} values are used to form the training sequences $X_1, X_2, \ldots, X_N$ and corresponding outputs $D_1, D_2, \ldots, D_N$. The weight matrices $M_W^1 (w_{ij})_{11*15}$ and $M_W^2 (w_{ij})_{15*7}$ from the input to hidden layers and hidden to output layers, respectively, are obtained by using the ANN training process in the MATLAB Neural Network Toolbox. The ANN based FBS coverage self-optimization is then applied to the randomly deployed FBS environments. The errors between the ANN based FBS coverage self-optimization and the target output value are shown in Figure 3.11, which shows the accuracy and effectiveness of the proposed scheme for FBS in different locations.
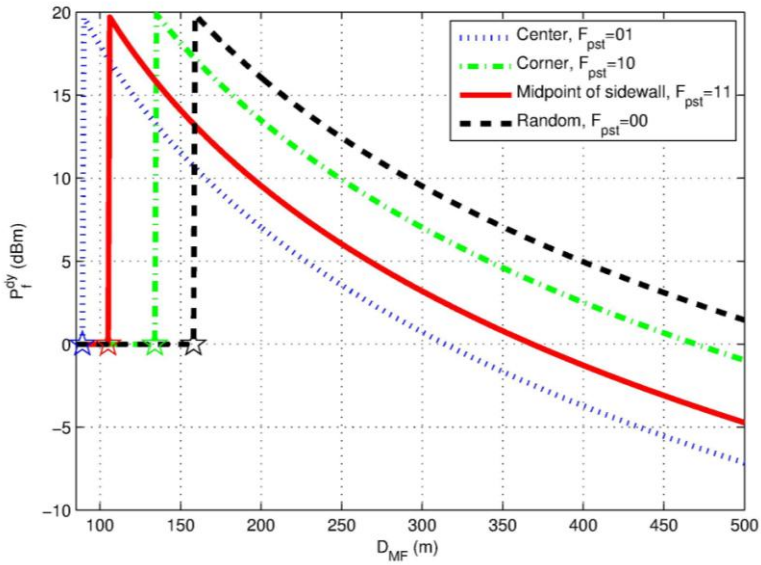
Table 3.2 *FBS parameters for coverage self-optimization. SOURCE: Reproduced with permission from [33]. Copyright 2015 Springer US.*

| F_{pst}	01	10	11	00
FBS position	Center	Corner	Sidewall	Random
A_i^p	01	10	11	00
Antenna pattern	Omni	90∘	180∘	Omni
FBS coverage radius R_f (m)	5.4	10.8	7.1	14.1
MBS interference range d_A (m)	83	123	97	143
Minimum distance $D_{MF}^{\min}$ (m)	89	134	105	158
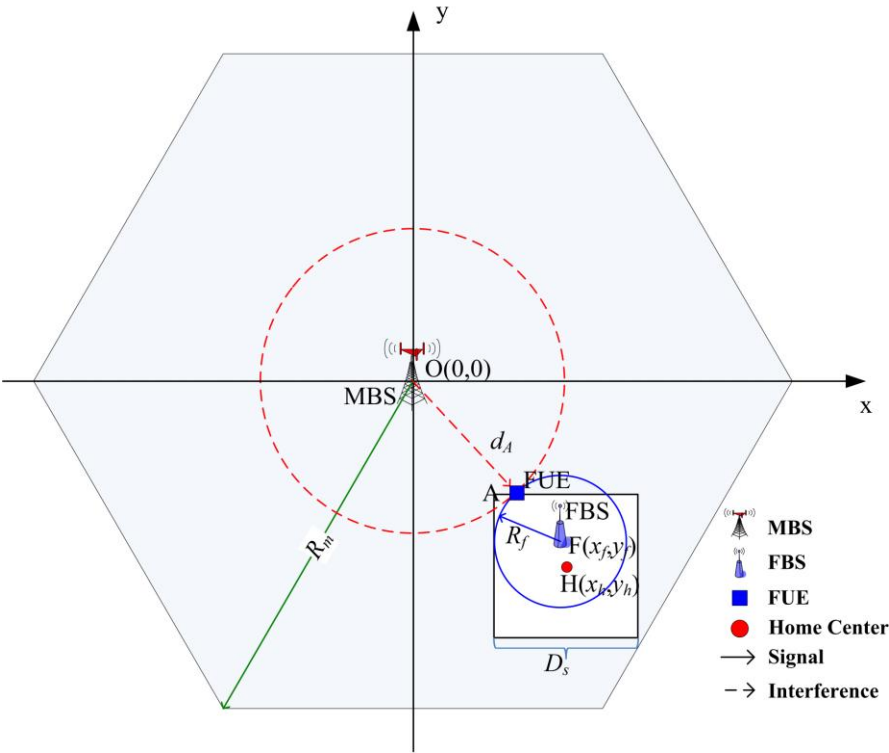
Figure 3.9 *FBS coverage self-optimization simulation environment. SOURCE: Reproduced with permission from [33]. Copyright 2015 Springer US.*

Figure 3.10 P_f^{dy} *versus* D_{MF} *for different FBS positions. SOURCE: Reproduced with permission from [33]. Copyright 2015 Springer US.*
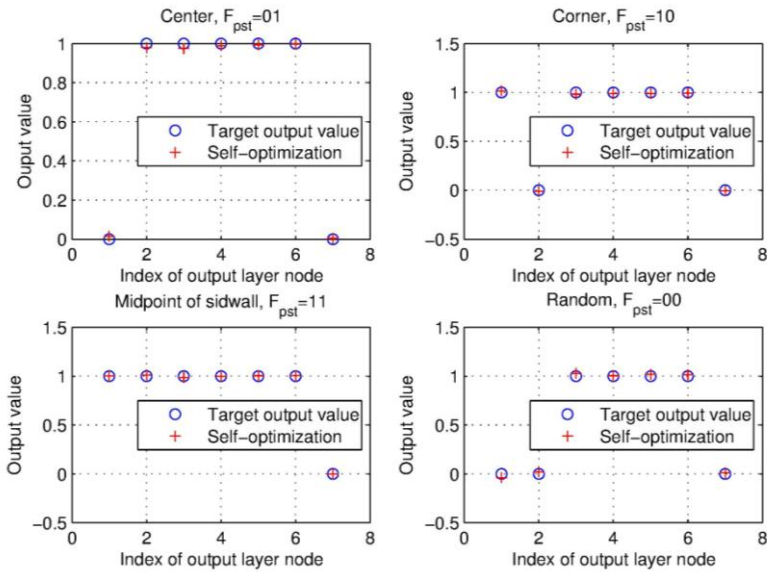
Figure 3.11   *ANN based FBS coverage self-optimization performance results for four different FBS locations. SOURCE: Reproduced with permission from [33]. Copyright 2015 Springer US.*

3.6 Concluding Remarks

Randomly deployed femtocell base stations (FBSs) have been examined in the indoor environment by considering outdoor interferences. A joint coverage self-optimization scheme has been developed and described in detail. The optimal coverage radii of FBS in typical positions, namely center, corner, and midpoint of the sidewall, are derived with closed-form results. Moreover, both static and dynamic power allocation schemes for FBS coverage optimization are analyzed and compared thoroughly. The position awareness between FBS and MBS is employed to obtain the joint antenna pattern selection and dynamic power allocation using the ANN model to realize the intelligent coverage self-optimization. Numerical results verify the effectiveness of the proposed coverage self-optimization scheme for randomly deployed FBSs.

References

[1] G. Mansfield, "Femtocells in the US market-business drivers and consumer propositions", *Femtocells Europe*, ATT, London, 2008.

[2] J. Cullen, "Radioframe presentation", *Femtocell Europe*, London, 2008.

[3] J. Zhang, G. de la Roche, "Femtocells: technologies and deployment", Wiley, New York, 2010.

[4] A. A. M. Saleh, A. Rustako and R. Roman, "Distributed antennas for indoor radio communications", *IEEE Trans. Commun.*, vol. 35, no. 12, pp. 1245-1251, Dec. 1987.

[5] A. Edwards, "The future is femto - [comms femtocells]", *IET Eng. Tech.*, vol. 3, no. 15, pp. 70-73, Sept. 2008.

[6] V. Chandrasekhar, J. G. Andrews and A. Gatherer, "Femtocell networks: a survey", *IEEE Commun. Mag.*, vol. 46, no. 9, pp. 59-67, Sept. 2008.

[7] Femtoforum, http://www.femtoforum.org.

[8] V. Chandrasekhar and J. G. Andrews, "Spectrum allocation in tiered cellular networks", *IEEE Trans. Commun.*, vol. 57, no. 10, pp. 3059-3068, Oct. 2009.

[9] D. Lopez-Perez, A. Valcarce, G. de la Roche and J. Zhang, "OFDMA femtocells: A roadmap on interference avoidance", *IEEE Commun. Mag.*, vol. 47, no. 9, pp. 41-48, Sept. 2009.

[10] H. Claussen, L. T. W. Ho and L. G. Samuel, "Self-optimization of coverage for femtocell deployments", *in Proc. IEEE WTS*, Pomona, CA, pp. 278-285, Apr. 2008.

[11] Ashraf, H. Claussen and L. T. W. Ho, "Distributed radio coverage optimization in enterprise femtocell networks", *in Proc. IEEE ICC*, Cape Town, pp. 1-6, May 2010.

[12] A. Barbieri et al, "LTE femtocells: system design and performance analysis", *IEEE J. Sel. Areas Commun.*, vol. 30, no. 3, pp. 586-594, Apr. 2012.

[13] H. Yun and K. G. Shin, "Adaptive interference management of OFDMA femtocells for co-channel deployment", *IEEE J. Sel. Areas Commun.*, vol. 29, no. 6, pp. 1225-1241, Jun. 2011.

[14] V. Chandrasekhar, J. G. Andrews, T. Muharemovic, Z. Shen and A. Gatherer, "Power control in two-tier femtocell networks", *IEEE Trans. Wireless Commun.*, vol. 8, no. 8, pp. 4316-4328, Aug. 2009.

[15] M. Yavuz et al, "Interference management and performance analysis of UMTS/HSPA+ femtocells", *IEEE Commun. Mag.*, vol. 47, no. 9, pp. 102-109, Sept. 2009.

[16] H. S. Jo, C. Mun, J. Moon and J. G. Yook, "Interference mitigation using uplink power control for two-tier femtocell networks", *IEEE Trans. Wireless Commun.*, vol. 8, no. 10, pp. 4906-4910, Oct. 2009.

[17] N. Arulselvan, V. Ramachandran, S. Kalyanasundaram and G. Han, "Distributed power control mechanisms for HSDPA femtocells", *in Proc. IEEE VTC Spring*, Barcelona, pp. 1-5. Apr. 2009.

[18] H. Claussen, "Performance of macro- and co-channel femtocells in a hierarchical cell structure", *in Proc. IEEE PIMRC*, Athens, pp. 1-5, Sept. 2007.

[19] T. W. Ho and H. Claussen, "Effects of user-deployed, co-channel femtocells on the call drop probability in a residential scenario", *in Proc. IEEE PIMRC*, Athens, pp. 1-5, Sept. 2007.

[20] D. N. Knisely, T. Yoshizawa and F. Favichia, "Standardization of femtocells in 3GPP", *IEEE Commun. Mag.*, vol. 47, no. 9, pp. 68-75, Sept. 2009.

[21] D. N. Knisely and F. Favichia, "Standardization of femtocells in 3GPP2", *IEEE Commun. Mag.*, vol. 47, no. 9, pp. 76-82, Sept. 2009.

[22] H. Claussen and F. Pivit, "Femtocell coverage optimization using switched multi-element antennas", *in Proc. IEEE ICC*, Dresden, pp. 1-6, Jun. 2009.

[23] V. Chandrasekhar, M. Kountouris and J. G. Andrews, "Coverage in multi-antenna two-tier networks", *IEEE Trans. Wireless Commun.*, vol. 8, no. 10, pp. 5314-5327, Oct. 2009.

[24] J. She, S. Q. Suo, H. Y. Quan, *3GPP Long Term Evolution: principle and system design*, Posts & Telecom Press, 2008.

[25] A. Goldsmith, *Wireless communications*, Cambridge University Press, 2005.

[26] Tsagkaris, A. Katidiotis, P. Demestichas, "Neural network-based learning schemes for cognitive radio systems", *Computer Commun.*, vol. 31, no. 14, pp. 3394-3404, 2008.

[27] J. J. Hopfield, "Artificial neural networks", *IEEE Circuits and Devices Mag.*, vol. 4, no. 5, pp. 3-10, 1998.

[28] G. Cybenko, "Approximation by superposition of sigmoidal functions", *Math. Control Signals and Systems*, pp. 303-314, 1989.

[29] S. Haykin, *Neural Networks and Learning Machines*, 3rd ed. Prentice Hall, Upper Saddle River, NJ, 2009.

[30] T. Hagan, H. B. Demuth, M. H. Beale, *Neural network design*, PWS Publishing, Boston, MA, 1996.

[31] T. Chen, H. Chen and R. W. Liu, "Approximation capability in $C(R^{-n})$ by multilayer feedforward networks and related problems", *IEEE Trans. Neural Networks*, vol. 6, no. 1, pp. 25-30, Jan. 1995.

[32] K. M. Mornik, M. Stinchcombe, H. White, "Multilayer feedforward networks are universal approximators", *Neural Networks*, vol. 2, no. 5, pp. 359-366, 1989.

[33] Q. Zhang, Z. Feng, Z. Wei, "Coverage self-optimization for randomly deployed femtocell networks", *Wireless Pers. Commun.*, vol. 82, no. 4, pp. 2481-2504, 2015.